A Compact Design for a Switchable Wireless Charger

WANG H.S.[1] CHENG K.W.E.[2] HU J.F.[3]

[1,2] Power Electronics Research Centre, Department of Electrical Engineering, The Hong Kong Polytechnic University, Hong Kong
[3] School of Engineering, Information Technology and Physical Sciences, Federation University, Australia
[1]E-mail: herschel.wang@connect.polyu.hk

Abstract –With the continuous miniaturization of electronic products, the compact structure of wireless power transfer (WPT) is extraordinarily necessary for consumer electronics. In addition, to meet the need in charging, load independent output current (CC) and constant output voltage (CV) are supposed to be taken into consideration since it is regarded as one of the most popular methods for charging batteries. This paper studies a switchable and compact design for a wireless charger. The compensation network can be changed between double LCL topology and LCL-S topology. Configurable CC and CV outputs can be achieved by adopting two switches without utilizing sophisticated control loops or any communication between the transmitter and the receiver. Compared with LCC compensation networks, the proposed special structure can save components under both double LCL and LCL-S conditions. The ferrite cores naturally take the responsibility as magnetic shielding for unwanted couplings in a such compact structure. This special design not only greatly alleviates the cross-coupling phenomenon but surely makes the compensation networks design straightforward as well. Ultimately, the fundamental analysis, the related mathematical derivation, detailed circuit topologies, switchable compensation designs and the experimental platform are all discussed and investigated. The proposed design is also analyzed and validated by experimental tests under different charging conditions.

Keywords – Wireless charging, inductive power transfer, compensation topology, switchable network, constant output

I. INTRODUCTION

Wireless power transfer (WPT) becomes increasingly attractive from researchers and engineers owing to its impressive benefits. For example, energy can be transferred without any mechanical contact over a relatively large gap. In other words, WPT can help electrical appliances gain energy without considering about the environmental surroundings. Energy can be transferred wirelessly through many materials such as air, water, wood, rock, etc. WPT have been successfully integrated with a great number of research areas such as the induction heating [1], the bidirectional charging [2], electric vehicles (EVs) [3], novel magnetic structures [4], power-data-parallel transmission [5] and the coil design [6], etc.

In general, WPT can be separated into far-field and near-field WPT according to the transmission distance. The far-field WPT can be formed through energy carriers like the acoustic, the optical, and the microwave [7]. Lately, near-field plays an important role in EVs as well as consumer electronics such as smart phones, laptops, the intelligent watch and earphones. There are two dominant types for near-field WPT, namely, capacitive power transfer (CPT) and inductive power transfer (IPT) [8]. Usually, CPT makes use of the electric field from capacitive metal plate couplers, resulting in a superior capability to penetrate through metal materials that already exist in the transmission path [9, 10]. By contrast, IPT system generally takes advantage of high-frequency magnetic fields generated by coils. Coils can also be designed delicately for various charging purposes. In recent years, IPT becomes more and more mature thanks to latest developments in magnetic materials: LITZ wire, embedded controllers, and high-frequency power electronics [11, 12].

In this paper, only IPT is discussed since it tends to be more commercially attractive compared to CPT. One extremely popular charged objective is the battery since they are universally utilized in smart phones, EVs, unmanned aerial vehicles (UAVs), and many other consumer electronics. Moreover, high-quality batteries can also be integrated with microgrids [13] and alternative energy device such as solar photovoltaics [14]. Fig. 1 illustrates a typical charging profile. The charging process begins with the CC mode. As the voltage of the battery jumps to a stable stage, the charger goes into CV mode until the charging current declines to zero approximately [15]. However, during the period of battery charging, the equivalent resistance of a battery tends to be roughly varied from a few ohms to several hundred ohms [16]. Hence, the load-independent CC and CV are required to against the load variation. There are several methods to fulfill battery charging requirements with a WPT system. One popular means is to put a dc-dc converter to regulate the output value either at the source side or the load side [17]. However, complicated control methods are needed to control the bulky dc-dc converters [18].

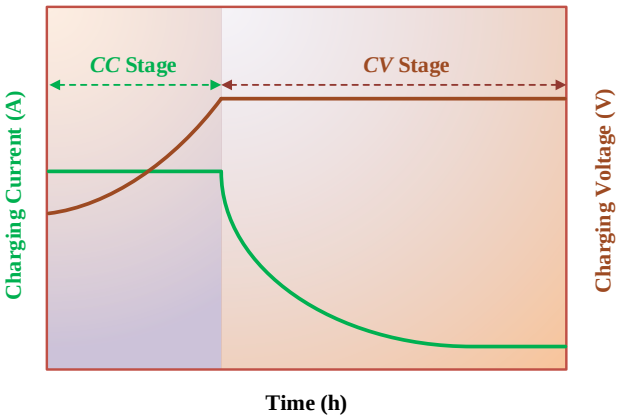

Fig. 1: The charging profile for the lithium-ion battery with CC and CV stages

Then, passive components are introduced to avoid complex control system and boost the simplicity. Well-organized compensation network can accomplish load-independent constant outputs including CC and CV,

minimize VA rating and maximized power transfer capability, suppress bifurcation phenomenon and enhance the efficiency [19]. Basically, four compensation topologies including SS, SP, PS and PP are widely used in two-coil WPT [20] as shown in Fig. 2 (a)-(d). Recently, several high-order compensation topologies such as LCL and LCC become more and more interesting owing to their special capabilities.

As illustrated in Fig. 2 (e), LCL topologies are proposed due to several advantages. Firstly, the primary current is able to be regardless of the reflected impedance from the secondary side [21]. Secondly, LCL topologies are studied to improve misalignment tolerance and lower voltage stresses across compensation capacitors [22].

As demonstrated in Fig. 2 (f), LCC topology is composed of inductor-capacitor-capacitor structure both on the transmitter and receiver side. This topology can accomplish ZCS [23] and the inverter only requires to provide the active power with a primary-side load-independent current [24].

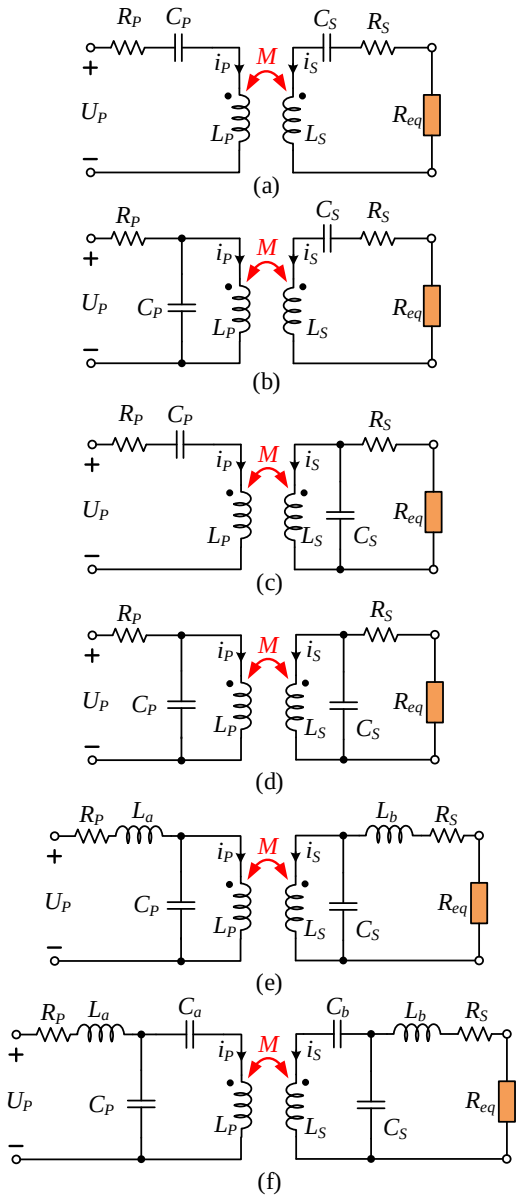

Fig. 2: Compensation topologies
(a) SS (b) PS (c) SP (d) PP (e) LCL (f) LCC

In addition, when it comes to existing wireless chargers, the communication from the receiver to the transmitter is often needed to build a closed-loop control to achieve the switch between CC and CV outputs. Nevertheless, wireless communication equipment tends to increase the system cost [25]. Furthermore, the wireless communication sometimes suffers from the interference created by the high-frequency magnetic field between the transmitter side and the receiver side. Especially, this may give rise to some problems like interruption or delay in some compact structures.

Therefore, a compact and switchable method is studied and built to resolve problems mentioned above. The key contributions are the following.

1) *Load-independent Outputs*: The load-independent CC and CV characteristics can be achieved by reconfiguring the circuit without any communication from the receiver to the transmitter. The system works in the CC mode within double LCL topology while CV mode within LCL-S topology.

2) *Simplicity and Reliability*: Only passive compensation topologies are used to regulate outputs. Without dc-dc converters, complicated control loops and corresponding interruption can be avoided. By eliminating the communication between the source and the load side, the proposed structure not only saves cost but also improves the robustness of the whole system.

3) *Compact Structure*: Without additional capacitors, pure LCL is more suitable for a compact structure. Besides, there is no need to put additional inductors far away from the main coupler to diminish unwanted couplings. Through inserting two ferrite cores, the unwanted couplings are greatly reduced while the major magnetic coupling from the transmitter and the receiver is enhanced. Moreover, the design of compensation networks can become more straightforward without considering unwanted couplings.

Nevertheless, the pure LCL structures give rise to the difficulty in designing magnetic couplers. Hence, finite element analysis (FEA) is used to well organize the proposed coupler. Detailed coupler design is demonstrated in section II. Section III provides fundamental analysis according to various circuits correspondingly. Section IV presents the experimental results with detailed hardware design and Section V concludes the whole paper.

II. Coupler Design

B. Coupler structure with detailed dimension

Fig. 3 depicts the proposed coupling structure including four spiral coils, i.e., L_a, L_P, L_S and L_b acting as the primary additional inductor, the transmitter coil, the receiver coil and the secondary additional inductor, respectively. For the compact purpose, the L_b and L_S are placed on upper surface and lower surface of ferrite core A,

respectively. Likewise, L_P and L_a are installed on upper surface and lower surface of ferrite core B, respectively.

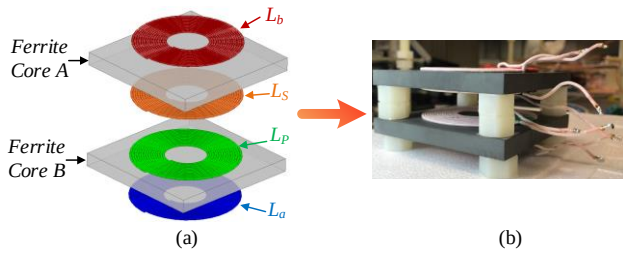

Fig. 3: The expanded and manufactured view of proposed coupler structure (a) Expanded view (b) Manufactured view

As illustrated in Fig. 4, the shape and size of these four coils are almost identical. And they are all manufactured by high-quality 140-strand LITZ wire. The external diameter of coils is 80mm while the inner diameter is 30mm. Then, ferrite cores are purely square-shaped (100mm×100mm). The size of ferrite cores is designed to be slightly larger than the corresponding size of coils, which offers better magnetic shielding for unwanted couplings. The transmission distance between T_X and R_X is 20mm.

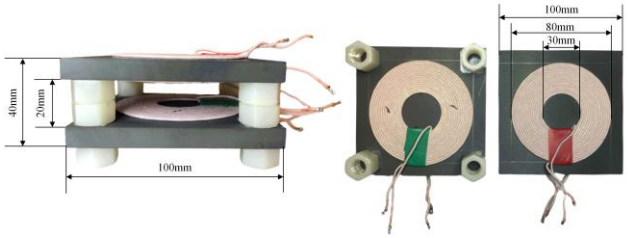

Fig. 4: Manufactured coupler structure with detailed dimension

B. Simulation results

The magnetic field distribution can be gained from finite element analysis software, which can be seen in Fig. 5. In this simulation, only the primary auxiliary coil L_a is excited to observe the magnetic field distribution directly. Fig. 5 depicts that the magnetic field generated from L_a mainly have the linkage with itself. That means the unwanted coupling from L_a is shielded by ferrite cores. There is no need to put L_a far away from the main coupling structure as conventional practice, contributing to a compact and concise configuration. Due to the symmetry of this design, the unwanted coupling from L_b is also greatly reduced from the same reason. Thus, only the major coupling k takes effects in this paper.

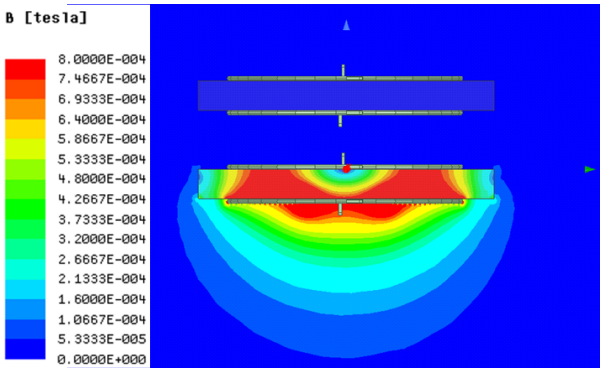

Fig. 5: A brief simulation result of the magnetic field

III. Fundamental Analysis

The entire scheme of the proposed WPT circuit model is demonstrated in Fig. 6. The primary DC voltage V_{dc} offered by DC power supply GP-1305DU from EZ Digital. The entire system is divided into two sides, i.e., the primary side through transmitter coil (T_X) and the secondary side through the receiver coil (R_X).

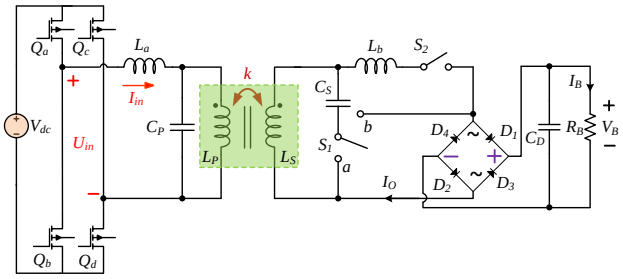

Fig. 6: The entire scheme of the proposed WPT circuit model

Ferrite cores made of material PC40 are used to enhance the magnetic coupling between T_X and R_X as a compact structure. The coupling coefficient k can be expressed as

$$k = \frac{M}{\sqrt{L_P \cdot L_S}} \tag{1}$$

where L_P and L_S are the self-inductances from T_X and R_X respectively and M is the mutual inductance between them. Due to the exist of ferrite cores, the unwanted coupling among L_a, L_b, R_X and T_X are all limited to an ignorable magnitude compared with the major coupling k between T_X and R_X. Next, V_B, I_B and R_B represent the voltage, current and the equivalent resistance of the battery, respectively.

The designed transmission distance is 2cm through the air from T_X to R_X. Then, the primary converter is a H-bridge inverter that is mainly composed of Q_a, Q_b, Q_c *and* Q_d. The secondary converter is a diode bridge rectifier (D_1, D_2, D_3, D_4 and C_D). The equivalent series resistances (ESRs) from the primary and secondary sides are neglected for simplification.

In terms of the inverter, its output voltage with 300ns dead time. Next, the root mean square (RMS) value of the β_{th} order harmonic component from the inverter output voltage u_{in} can be expressed as [26]

$$U_{in\_\beta} = \frac{2\sqrt{2}}{\beta\pi} V_{dc} (\beta = 1,3,5,7,9\ldots) \tag{2}$$

Because the high-order resonant circuit works as bandpass filters, higher order harmonics are mainly filtered out [26]. In this paper, only the fundamental component is taken into account for the sake of simplification and it can be written as [27].

$$\dot{U}_{in} = \frac{2\sqrt{2}V_{dc}}{\pi} \angle 0^{\circ} \tag{3}$$

As for the rectifier, the relationship between its input and output value can be shown as

$$U_O = \frac{2\sqrt{2}}{\pi} V_B \tag{4}$$

$$I_O = \frac{\pi}{2\sqrt{2}} I_B \tag{5}$$

R_{eq}, the equivalent load of the rectifier [28], can be gained as

$$R_{eq} = \frac{8}{\pi^2} R_B \tag{6}$$

Therefore, the rectifier part from Fig. 6 can be replaced by the equivalent load for simplification. The simplified diagram of the proposed WPT circuit model is illustrated in Fig. 7, where U_O and I_O are the input voltage and current value of the rectifier, respectively. Two switches, namely, S_1 and S_2 are used for the switching between CC and CV stages. S_1 works as a single-pole double-throw switch while S_2 acts as a single-pole single-throw switch. The configuration can be re-arranged through switches. Detailed information is shown as follows.

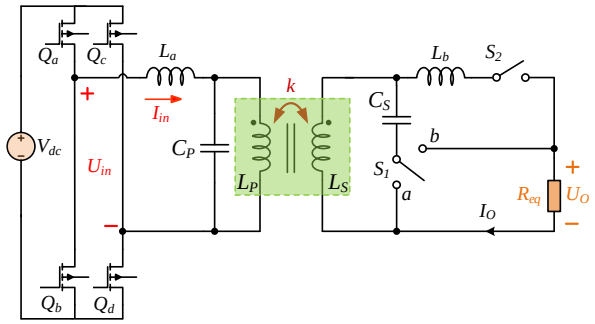

Fig. 7: The simplified diagram of the proposed WPT circuit model

A. The analysis of double LCL configuration for CC stage

As shown in Fig. 8, the circuit of the double LCL configuration is constructed when the switch S_1 is thrown to the terminal *a* as well as the S_2 is switched on. L_a, L_b, C_P and C_S are the auxiliary inductors and the resonant capacitors in the primary side and secondary side, respectively. For tuning the coils, the operating angular frequency of the inverter ω needs to meet the following equation:

$$\omega = \sqrt{\frac{1}{L_a C_P}} = \sqrt{\frac{1}{L_P C_P}} = \sqrt{\frac{1}{L_S C_S}} = \sqrt{\frac{1}{L_b C_S}} \tag{7}$$

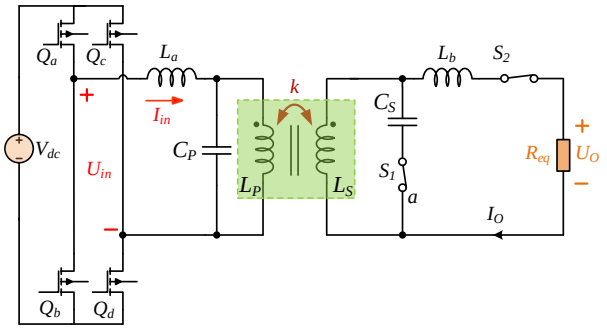

Fig. 8: The scheme of the double LCL WPT system

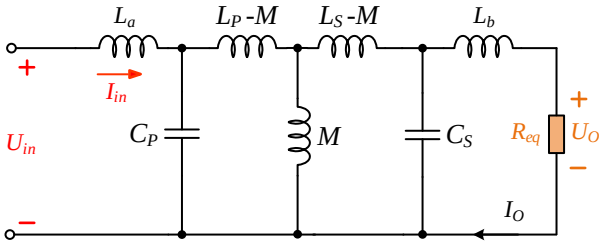

Fig. 9: The equivalent T-model of the double LCL WPT system

The equivalent T-model of the double LCL WPT system is demonstrated in Fig. 9. Through the conversion of the resonant circuits, the relationship between the input and output can be expressed as

$$\dot{I}_O = \frac{M}{j\omega L_S L_a} \dot{U}_{in} \tag{8}$$

Substituting (3) and (5) into (8), we can get

$$I_B = \frac{8M}{\pi^2 \omega L_S L_a} V_{dc} \tag{9}$$

Therefore, the current of the battery is independent of the load. A load-independent CC from the wireless charger can be gained through this double LCL configuration.

B. CV stage with LCL-S configuration

As shown in Fig. 10, the circuit of the double LCL configuration is constructed when the switch S_1 is thrown to the terminal *b* as well as the S_2 is switched off. L_a, L_b, C_P and C_S are the auxiliary inductors and the resonant capacitors in the primary side and secondary side, respectively. Similarly, ω should meet the following equation for tuning the coils.

$$\omega = \sqrt{\frac{1}{L_a C_P}} = \sqrt{\frac{1}{L_P C_P}} = \sqrt{\frac{1}{L_S C_S}} \tag{10}$$

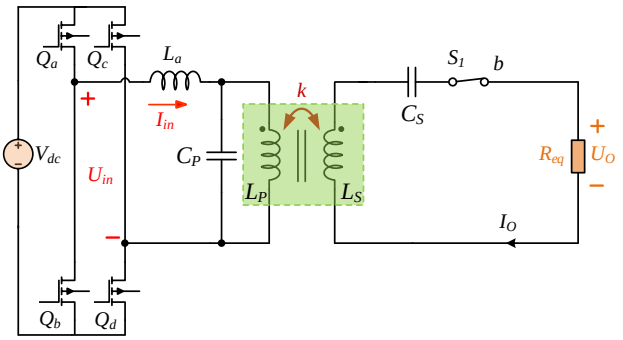

Fig. 10: The scheme of the LCL-S WPT system

The equivalent T-model of the LCL-S configuration is illustrated in Fig. 11. Through the conversion of the resonant circuits, the relationship between the input and output can be gained as

$$\dot{U}_O = \frac{M}{L_a} \dot{U}_{in} \tag{11}$$

Similarly, substituting (3) and (4) into (11), we can get

$$V_B = \frac{M}{L_a} V_{dc} \tag{12}$$

Thus, the voltage of the battery V_B is independent of the load. A load-independent CV from the wireless charger can be gained through this LCL-S configuration.

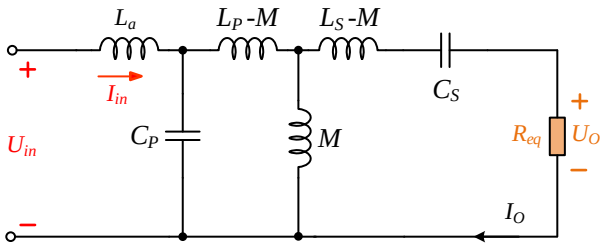

Fig. 11: The equivalent T-model of the LCL-S WPT system

IV. Experimental Verification

An experimental platform has been built up to verify the theoretical analysis as demonstrated in Fig. 12. The operating frequency from the inverter *f* is fixed as 200kHz. The battery is replaced by two resistive loads for simplification. There is a switch equipped with these two resistances for the dynamic response test when the load change happens. Experimental waveforms are directly gained and analysed from oscilloscope Tektronix MDO3024. The two output channels from power supply EZ Digital GP-1305DU are connected in series to power the inverter. The maximum output of this DC power supply device is approximately 60V. Two switches, namely, S_1 and S_2 are used to turn on/off specific loops. Measured parameters from this prototype can be found in Table. 1.

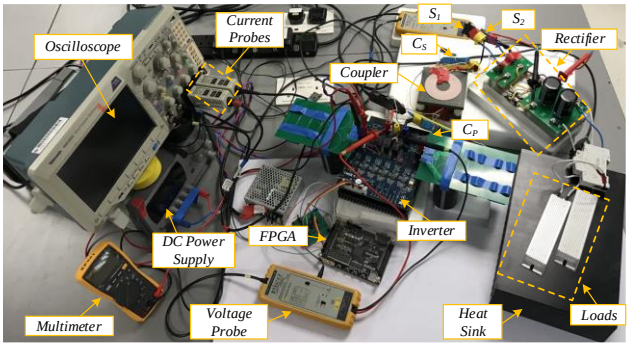

Fig. 12: The whole experimental prototype

Table 1: Measured parameters

L_a	L_P	L_S	L_b
23.79μH	24.02μH	23.85μH	24.01μH
M	C_P	C_S	f
12.32μH	26.03nF	26.19nF	200kHz

A. Experimental results of the double LCL configuration

Fig. 13 depicts the essential waveforms from the inverter and the output information at the load side. This inverter output current slightly lags the inverter output voltage, which reveals ZVS can be ensured through the double LCL configuration.

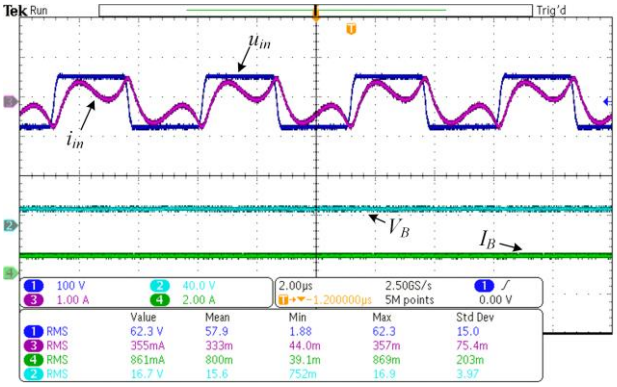

Fig. 13: Essential waveforms from the inverter, the output voltage and current on the load in double LCL configuration

Fig. 14 illustrates the dynamic response during the process that the load is changed from 20Ω to 40Ω and then from 40Ω to 20Ω. The switching points are manifested by the dotted ellipse. The voltage variation is 16.8V that can be directly detected by the oscilloscope. However, the current on the load keeps at 880mA with slight overshoots as shown in Fig. 15, which verifies the CC characteristic from the double LCL configuration.

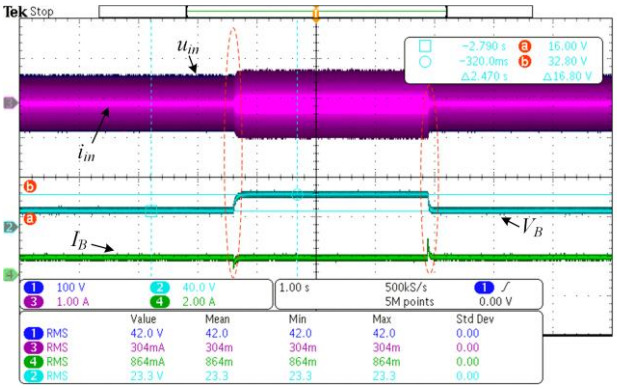

Fig. 14: Dynamic response with voltage data when the load changes from 20Ω to 40Ω and back to 20Ω in double LCL type

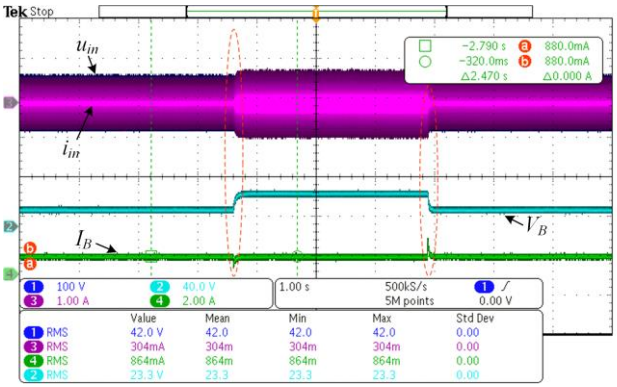

Fig. 15: Dynamic response with current data when the load changes from 20Ω to 40Ω and back to 20Ω in double LCL type

B. Experimental results of the LCL-S configuration

Fig. 16 describes the essential waveforms from the inverter and the output data from the load side. This inverter output current slightly lags the inverter output voltage, which shows this LCL-S configuration can achieve ZVS.

The dynamic response of LCL-S type can be observed from Fig. 17 during the process that the load is switched between 20Ω and 40Ω. The switching points are

manifested by the dotted ellipse too. The change of load current is 800mA, which can be directly detected through the oscilloscope. However, the voltage on the load keeps stable at 30.4V as illustrated in Fig. 18 when load variation happens, which validates the CV characteristic from the LCL-S configuration.

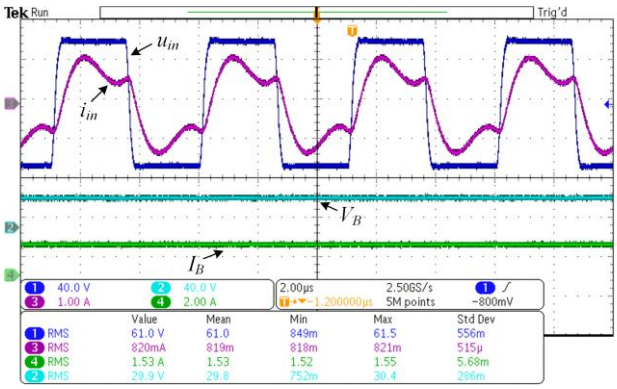

Fig. 16: Essential waveforms from the inverter, the output voltage and current on the load in LCL-S type

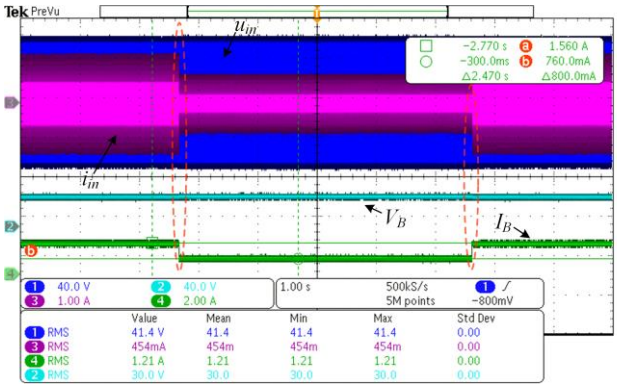

Fig. 17: Dynamic response with current data when the load changes from 20Ω to 40Ω and back to 20Ω in LCL-S type

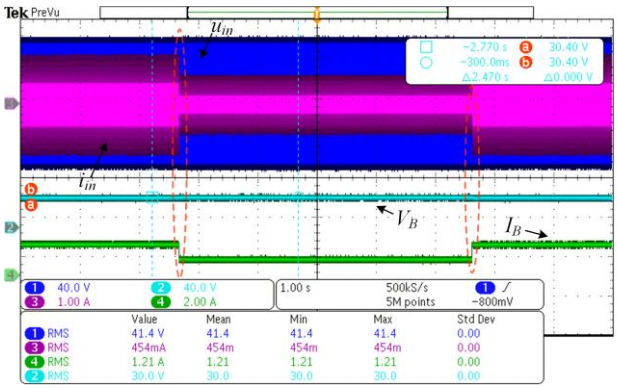

Fig. 18: Dynamic response with voltage data when the load changes from 20Ω to 40Ω and back to 20Ω in LCL-S type

V. Conclusion

A compact design for a switchable wireless charger is investigated in this paper. Special magnetic coupler equipped with ferrite cores are proposed to enhance the major coupling between T_X and R_X as well as to reduce the unwanted cross-couplings simultaneously. By doing this, the coupling coefficient between T_X and R_X is improved and the compensation networks can be designed straightforward. Key characteristics such as ZVS, load-independent CC and CV are demonstrated through essential waveforms. In particular, the fundamental analysis, the mathematical derivation, detailed circuit analysis, compensation network designs are all discussed and studied. An experimental prototype is built to evaluate the performance and related test results successfully show the agreement with the analysis. The design in this paper can be adjusted in size to meet the needs of different IPT systems for wirelessly charging smart phones, UAVs, or EVs.

References

[1] L. Meng and K. W. E. Cheng, "Wireless power transfer technology for electric iron based on multi-coils induction heating design," *IET Power Electronics*, vol. 12, no. 10, pp. 2566-2577, 2019.

[2] Y. C. Fong and K. W. E. Cheng, "A switched-capacitor step-up inverter for bidirectional wireless charging applications in electric microcar," in *2017 7th International Conference on Power Electronics Systems and Applications - Smart Mobility, Power Transfer & Security (PESA)*, 12-14 Dec. 2017 2017, pp. 1-6,

[3] K. W. K. Chen and K. W. E. Cheng, "Review of magnetic resonance technology, recent research trends and issues in EV wireless charging," in *The 11th IET International Conference on Advances in Power System Control, Operation and Management (APSCOM 2018)*, 11-15 Nov. 2018 2018, pp. 1-7,

[4] M. Chen, E. K. Cheng, and J. Hu, "Near Field Wireless Power Transfer for Multiple Receivers by Using a Novel Magnetic Core Structure," in *2018 IEEE Energy Conversion Congress and Exposition (ECCE)*, 23-27 Sept. 2018 2018, pp. 1190-1195,

[5] X. Li, J. Hu, Y. Li, H. Wang, M. Liu, and P. Deng, "A Decoupled Power and Data-Parallel Transmission Method With Four-Quadrant Misalignment Tolerance for Wireless Power Transfer Systems," *IEEE Transactions on Power Electronics*, vol. 34, no. 12, pp. 11531-11535, 2019.

[6] Y. Li *et al.*, "A New Coil Structure and Its Optimization Design With Constant Output Voltage and Constant Output Current for Electric Vehicle Dynamic Wireless Charging," *IEEE Transactions on Industrial Informatics*, vol. 15, no. 9, pp. 5244-5256, 2019.

[7] Z. Zhang, H. Pang, A. Georgiadis, and C. Cecati, "Wireless Power Transfer—An Overview," *IEEE Transactions on Industrial Electronics*, vol. 66, no. 2, pp. 1044-1058, 2019.

[8] X. Mou and H. Sun, "Wireless Power Transfer: Survey and Roadmap," in *2015 IEEE 81st Vehicular Technology Conference (VTC Spring)*, 11-14 May 2015 2015, pp. 1-5,

[9] L. Huang, A. P. Hu, A. K. Swain, and Y. Su, "Z-Impedance Compensation for Wireless Power Transfer Based on Electric Field," *IEEE Transactions on Power Electronics*, vol. 31, no. 11, pp. 7556-7563, 2016.

[10] Y. Su, S. Xie, A. P. Hu, C. Tang, W. Zhou, and L. Huang, "Capacitive Power Transfer System With a Mixed-Resonant Topology for Constant-Current Multiple-Pickup Applications," *IEEE Transactions on Power Electronics*, vol. 32, no. 11, pp. 8778-8786, 2017.

[11] G. A. Covic and J. T. Boys, "Modern Trends in Inductive Power Transfer for Transportation Applications," *IEEE Journal of Emerging and Selected Topics in Power Electronics*, vol. 1, no. 1, pp. 28-41, 2013.

[12] G. A. Covic and J. T. Boys, "Inductive Power Transfer," *Proceedings of the IEEE*, vol. 101, no. 6, pp. 1276-1289, 2013.

[13] J. Hu, Y. Xu, K. W. Cheng, and J. M. Guerrero, "A model predictive control strategy of PV-Battery microgrid under variable power generations and load conditions," *APPL ENERG*, vol. 221, pp. 195-203, 2018.

[14] Y. Shan, J. Hu, K. W. Cheng, and M. Liu, "A Universal

Model Predictive Control for Practical AC Microgrids with PVs and Battery Energy Storage Systems," in *2018 IEEE Energy Conversion Congress and Exposition (ECCE)*, 23-27 Sept. 2018 2018, pp. 6257-6262,

[15] X. Qu, H. Han, S. Wong, C. K. Tse, and W. Chen, "Hybrid IPT Topologies With Constant Current or Constant Voltage Output for Battery Charging Applications," *IEEE Transactions on Power Electronics,* vol. 30, no. 11, pp. 6329-6337, 2015.

[16] G. Buja, M. Bertoluzzo, and K. N. Mude, "Design and Experimentation of WPT Charger for Electric City Car," *IEEE Transactions on Industrial Electronics,* vol. 62, no. 12, pp. 7436-7447, 2015.

[17] Y. Li, Y. Sun, and X. Dai, "/spl mu/-Synthesis for Frequency Uncertainty of the ICPT System," *IEEE Transactions on Industrial Electronics,* vol. 60, no. 1, pp. 291-300, 2013.

[18] C. Xia, W. Wang, G. Chen, X. Wu, S. Zhou, and Y. Sun, "Robust Control for the Relay ICPT System Under External Disturbance and Parametric Uncertainty," *IEEE Transactions on Control Systems Technology,* vol. 25, no. 6, pp. 2168-2175, 2017.

[19] W. Zhang and C. C. Mi, "Compensation Topologies of High-Power Wireless Power Transfer Systems," *IEEE Transactions on Vehicular Technology,* vol. 65, no. 6, pp. 4768-4778, 2016.

[20] Y. Wang, H. Wang, T. Liang, X. Zhang, D. Xu, and L. Cai, "Analysis and design of an LCC/S compensated resonant converter for inductively coupled power transfer," in *2017 IEEE Transportation Electrification Conference and Expo, Asia-Pacific (ITEC Asia-Pacific)*, 7-10 Aug. 2017 2017, pp. 1-5,

[21] H. Hao, G. A. Covic, and J. T. Boys, "An Approximate Dynamic Model of LCL- T-Based Inductive Power Transfer Power Supplies," *IEEE Transactions on Power Electronics,* vol. 29, no. 10, pp. 5554-5567, 2014.

[22] N. A. Keeling, G. A. Covic, and J. T. Boys, "A Unity-Power-Factor IPT Pickup for High-Power Applications," *IEEE Transactions on Industrial Electronics,* vol. 57, no. 2, pp. 744-751, 2010.

[23] Z. Pantic, S. Bai, and S. M. Lukic, "ZCS LCC-Compensated Resonant Inverter for Inductive-Power-Transfer Application," *IEEE Transactions on Industrial Electronics,* vol. 58, no. 8, pp. 3500-3510, 2011.

[24] S. Li, W. Li, J. Deng, T. D. Nguyen, and C. C. Mi, "A Double-Sided LCC Compensation Network and Its Tuning Method for Wireless Power Transfer," *IEEE Transactions on Vehicular Technology,* vol. 64, no. 6, pp. 2261-2273, 2015.

[25] Y. Li *et al.*, "Reconfigurable Intermediate Resonant Circuit Based WPT System With Load-Independent Constant Output Current and Voltage for Charging Battery," *IEEE Transactions on Power Electronics,* vol. 34, no. 3, pp. 1988-1992, 2019.

[26] Y. Li *et al.*, "Analysis, Design, and Experimental Verification of a Mixed High-Order Compensations-Based WPT System with Constant Current Outputs for Driving Multistring LEDs," *IEEE Transactions on Industrial Electronics,* vol. 67, no. 1, pp. 203-213, 2020.

[27] H. Cai, L. Shi, and Y. Li, "Harmonic-Based Phase-Shifted Control of Inductively Coupled Power Transfer," *IEEE Transactions on Power Electronics,* vol. 29, no. 2, pp. 594-602, 2014.

[28] Y. Li, Q. Xu, T. Lin, J. Hu, Z. He, and R. Mai, "Analysis and Design of Load-Independent Output Current or Output Voltage of a Three-Coil Wireless Power Transfer System," *IEEE Transactions on Transportation Electrification,* vol. 4, no. 2, pp. 364-375, 2018.